Remote Sensing of Environment 152 (2014) 51–61

Contents lists available at ScienceDirect

Remote Sensing of Environment

journal homepage: www.elsevier.com/locate/rse

Surface urban heat island in China's 32 major cities: Spatial patterns and drivers

Decheng Zhou [a], Shuqing Zhao [a,*], Shuguang Liu [b], Liangxia Zhang [c], Chao Zhu [a]

[a] College of Urban and Environmental Sciences, and Key Laboratory for Earth Surface Processes of the Ministry of Education, Peking University, Beijing 100871, China
[b] National Engineering Laboratory of Forest Ecology and Applied Technology for Southern China, and Central South University of Forest and Technology, Changsha 410004, China
[c] Institute of Geographic Sciences and Natural Resources Research, Chinese Academy of Sciences, Beijing 100101, China

ARTICLE INFO

Article history:
Received 7 November 2013
Received in revised form 23 May 2014
Accepted 26 May 2014
Available online 19 June 2014

Keywords:
urbanization
land surface temperature (LST)
spatial variations
driving forces
enhanced vegetation index (EVI)
albedo
climatic effects

ABSTRACT

Urban heat island (UHI) is a major anthropogenic alteration on Earth environments and its geospatial pattern remains poorly understood over large areas. Using MODIS data from 2003 to 2011, we quantified the diurnal and seasonal surface UHI intensity (SUHII, urban–suburban temperature difference) in China's 32 major cities, and analyzed their spatial variations and possible underlying mechanisms. Results show that the annual mean SUHII varied markedly from 0.01 to 1.87 °C in the day and 0.35 to 1.95 °C at night, with a great deal of spatial heterogeneities. Higher SUHIIs for the day and night were observed in the southeastern and northern regions, respectively. Moreover, the SUHII differed greatly by season, characterized by a higher intensity in summer than in winter during the day, and the opposite during the night for most cities. Consequently, whether the daytime SUHII was higher or lower than the nighttime SUHII for a city depends strongly on the geographic location and research period. The SUHII's distribution in the day related closely to vegetation activity and anthropogenic heat releases in summer, and to climate (temperature and precipitation) in winter, while that at night linked tightly to albedo, anthropogenic heat releases, built-up intensity, and climate in both seasons. Overall, we found the overwhelming control of climate on the SUHII's spatial variability, yet the factors included in this study explained a much smaller fraction of the SUHII variations in the day compared to night and in summer relative to winter (day vs. night: 57% vs. 72% in summer, and 61% vs. 90% in winter, respectively), indicating more complicated mechanisms underlying the distribution of daytime SUHII, particularly in summer. Our results highlight the different diurnal (day and night) and seasonal (summer and winter) SUHII's spatial patterns and driving forces, suggesting various strategies are needed for an effective UHI effect mitigation.

1. Introduction

Urbanization, a major human activity, poses increasingly strong impacts on Earth environments (Grimm et al., 2008; Vitousek, Mooney, Lubchenco, & Melillo, 1997). Among these effects, the resultant urban heat island (UHI), refers to the phenomenon that urban areas tend to have higher atmospheric or surface temperatures than the surroundings, is one of the most well-documented example of anthropogenic modification on Earth system (Arnfield, 2003; IPCC, 2007; Oke, 1973; Voogt & Oke, 2003). UHI can not only alter the eco-environments such as net primary production (Imhoff et al., 2004), biodiversity (Reid, 1998), water and air quality (Grimm et al., 2008), and climate (Arnfield, 2003; Dixon & Mote, 2003; IPCC, 2007; Jin, Dickinson, & Zhang, 2005; Jin, Shepherd, & King, 2005; Shepherd, 2005) but also affect human health and well-beings like an increase in morbidity, mortality, and risk of violence (Gong et al., 2012; O'Loughlin et al., 2012; Patz, Campbell-Lendrum, Holloway, & Foley, 2005). These impacts were expected to be more serious when interacting with global climate changes (IPCC, 2007; McCarthy, Best, & Betts, 2010; Patz et al., 2005). Thus, a better understanding of the UHI effects is critically important to support future climate mitigation actions and human adaptive strategies (Arnfield, 2003; Imhoff, Zhang, Wolfe, & Bounoua, 2010; Oke, 1973).

UHI has two broad types. The first is the atmospheric UHI calculated from weather station networks (Chow & Roth, 2006; Fast, Torcolini, & Redman, 2005; Karl & Quayle, 1988; Peterson, 2003) and the second is the surface UHI estimated from thermal infrared remote sensing techniques (Imhoff et al., 2010; Jin, Dickinson, et al., 2005; Peng et al., 2012; Voogt & Oke, 2003). Because of easy access and wall-to-wall coverage of satellite products, the surface UHI has gained rising attention in recent decades (Clinton & Gong, 2013; Imhoff et al., 2010; Jin, Dickinson, et al., 2005; Peng et al., 2012; Tran, Uchihama, & Yasuoka, 2006; Zhang, Imhoff, Wolfe, & Bounoua, 2010). We will deal with the surface UHI intensity (SUHII) in this study.

Surface UHI remains poorly understood over large areas. Most of the previous studies were conducted in a particular or several contrasting

* Corresponding author.
E-mail address: sqzhao@urban.pku.edu.cn (S. Zhao).

http://dx.doi.org/10.1016/j.rse.2014.05.017
0034-4257/

cities regarding the magnitude of surface UHI rather than geospatial patterns (e.g., Li et al., 2011; Tran et al., 2006; Yuan & Bauer, 2007). A few recent efforts had been made to understand the regional and global distributions of SUHII, yet they concentrated on big cities that are mostly situated in coastal areas and/or have different driving variables, therefore leading to highly diverse conclusions (Clinton & Gong, 2013; Imhoff et al., 2010; Jin, Dickinson, et al., 2005; Peng et al., 2012; Zhang et al., 2010). For instance, Jin, Dickinson, and Zhang (2005) suggested that the SUHII were pronounced at both daytime and nighttime globally but did not explore their drivers. Zhang et al. (2010) only focused on the daytime SUHII and the ecological control on global variations. Imhoff et al. (2010) demonstrated that the SUHII was more intense in the day than at night, and was mainly controlled by ecological context across 38 metropolises in the conterminous United States. Peng et al. (2012) also concluded that the SUHII was significantly higher in the day than at night across 419 global big cities and their spatial variability was attributed to the urban–suburban differences in vegetation activity during the daytime and in albedo and anthropogenic heat releases at night. The most recent global report (Clinton & Gong, 2013) indicated a similar magnitude for annual mean SUHII in the day and at night averaged across cities with large geographical heterogeneity that was mainly determined by the development intensity, vegetation amount, and the size of the urban metropolis. Apparently, a more detailed assessment on the spatial patterns of SUHII and underlying mechanisms is needed for a better understanding of the UHI effects over large areas.

Located in the East Asian monsoon region, China covers a wide temperature gradient decreasing from south to north and a large precipitation gradient decreasing from southeast to northwest (Wu, Yin, Zheng, & Yang, 2005), suggesting China should be an ideal place to examine the impacts of UHI at regional scale. Various studies have documented the SUHII in selected cities in China (Cai, Du, & Xue, 2011; Ding & Shi, 2013; Li et al., 2011; Tran et al., 2006; Xu & Chen, 2004). However, to our knowledge, no studies have systematically analyzed the SUHII of all major cities in China. Quantifying and analyzing the magnitude and spatial pattern of SUHII in China can not only help enhance understanding the physical characteristics, driving forces, and consequences of UHI in general, but also be essential for formulating climate mitigation strategies and plans in the country.

The purpose of this study was to investigate the geographic variations of the diurnal and seasonal SUHII in China's 32 major cities, and to explore their possible driving forces. The latest version 5 of Moderate Resolution Imaging Spectroradiometer (MODIS) Land Surface Temperature (LST) data were used to evaluate the surface temperature differences between urban and surrounding suburban areas over these 32 major cities that are distributed across China. Measurements of SUHII were related to both biophysical and anthropogenic factors to explore the possible causes for their spatial variabilities.

2. Data and methods

2.1. Datasets

We focused on 32 major cities in China (Fig. 1). All of them are municipalities or provincial capitals except Shenzhen, which is China's first special economic zone established in 1978 and is now considered as one of the fastest-growing cities around the world. To investigate the geographic variations of SUHII, these cities were grouped into six regions according to the geography of China (Fang, Chen, Peng, Zhao, & Ci, 2001): North China (Beijing, Hohhot, Shijiazhuang, Taiyuan, and Tianjin), Northeast China (Changchun, Harbin, and Shenyang), East China (Fuzhou, Hangzhou, Hefei, Jinan, Nanchang, Nanjing, and Shanghai), Central-south China (Changsha, Guangzhou, Haikou, Nanning, Shenzhen, Wuhan, and Zhengzhou), Southwest China (Chengdu, Chongqing, Guiyang, Kunming, and Lhasa), and Northwest China (Lanzhou, Urumqi, Xi'an, Xining, and Yinchuan) (Fig. 1). The east, central-south, and southwest parts of China have typical humid-hot climate. Northeast China, North China, and Northwest China have typical humid-cold, subhumid/semiarid-temperate, and arid climates, respectively (Wu et al., 2005).

Land surface temperature (i.e., LST) was obtained from Aqua MODIS 8-days composite products (version 5) with a spatial resolution of 1 km × 1 km (MYD11A2) from 2003 to 2011 for each city. The Aqua MODIS LST data was retrieved from clear-sky (99% confidence) observations that monitored at 1:30 and 13:30 local solar time using a generalized split-window algorithm (Wan & Dozier, 1996). Wan (2008) reported that the accuracy of MODIS V5 LST is better than 1 K for most tested cases (39 out of 47), and Rigo, Parlow, and Oesch (2006) found less than 5% differences between MODIS LSTs and in-situ measurements in urban areas.

Urban coverage map of each city was derived from the cloud-free Landsat TM/ETM + images (http://www.usgs.gov/ and http://datamirror.csdb.cn/) with a high spatial resolution of 30 m × 30 m in circa 2000, 2005, and 2010. First, the Landsat images were preprocessed (e.g., re-projection, mosaic, histogram equalization) using ERDAS Imagine version 9.2. Second, the land covers were grouped into three types (i.e., built-up land, water body, and other land) using the maximum likelihood classification approach (Strahler, 1980). Built-up land consisted of the impervious surfaces of cities, towns (lands used for townships and settlement), and industrial and mining lands. Water body represents the reservoirs, ponds, and rivers. Other land represents all the other kinds of land covers including cropland, forest, shrub, grass, and unused land. Finally, the accuracies of the classified products were assessed using Google Earth Pro® (GE) following the approach of Zhou, Zhao, and Zhu (2012), and the Kappa coefficients measuring classification accuracy (Foody, 2002) were calculated. Kappa coefficients for the 32 cities ranged from 0.77 to 0.93, with most of them were larger than 0.80, which meets the accuracy requirements of this analysis.

The following datasets were assembled to examine their relations with the SUHII:

a) The MODIS Enhanced Vegetation Index (EVI) (16-day composites) and Bidirectional Reflectance Distribution Function (BRDF) albedo (8-day composites) from 2003–2011: the albedo products consisted of shortwave black sky albedo (BSA, directional hemispherical reflectance at local solar noon) and white sky albedo (WSA, bihemispherical reflectance). Because the BSA was linearly correlated with WSA and showed a similar relationship with SUHII to WSA (Peng et al., 2012), only WSA was utilized in this analysis.
b) Digital Elevation Model (DEM): digital elevation data at a 3 arc-second (approximately 90 m) spatial resolution from the Space Shuttle Radar and Topography Mission (SRTM) was used (http://earthexplorer.usgs.gov/).
c) Built-up Intensity (BI): the BI, defined as the percentage of landscape taken by built-up land, was derived from urban coverage maps. Methods to derive BI will be described in 2.2. Analysis.
d) Climate information on temperature and precipitation: monthly climate data from 2003 to 2011 for each city was obtained from Chinese Meteorological Observations (http://cdc.cma.gov.cn/). The meteorological station for each city was located within its suburban or urban area to reflect the climatic background for each city (Fig. 1).
e) Nighttime lights: the remotely sensed nighttime light signals derived from the Defense Meteorological Satellite Program's Operational Linescan System (DMSP/OLS) (version 4 and downloaded from http://ngdc.noaa.gov/eog/dmsp/ downloadV4composites.html) were used to as a proxy of anthropogenic heat releases in both urban and suburbs following previous studies (Elvidge et al., 2001; Ghosh et al., 2010; Peng et al., 2012). The annual DMSP data were compiled for 2003–2010 with a nominal spatial resolution of 2.7 km.

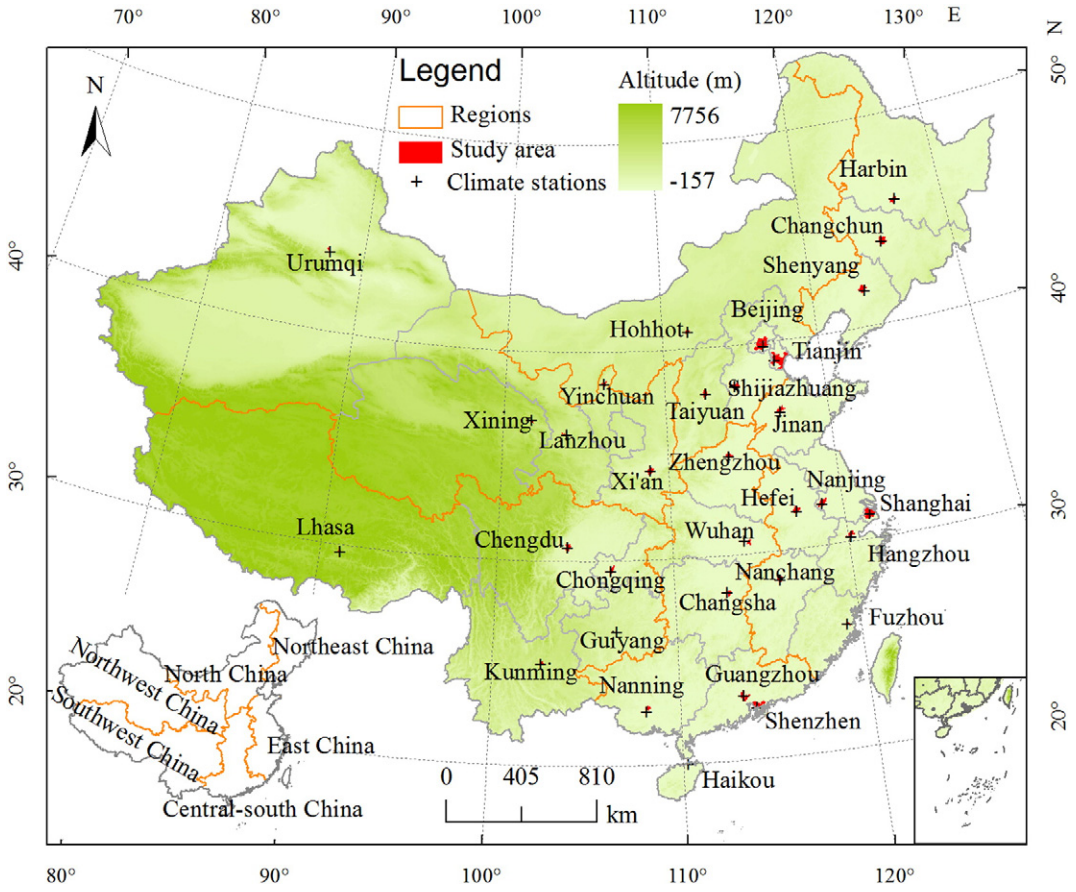

Fig. 1. Locations of the 32 major cities and six regions in China, with the background map indicating the topography of China. All of the cities are municipalities or provincial capitals except Shenzhen, which is China's first special economic zone established in 1978, and is now considered one of the fastest-growing cities in the world. The meteorological station for each city located within its suburban or urban area to reflect the climatic background for each city was showed as well.

2.2. Analysis

In this study, the SUHII was defined as the LST difference between urban and its surrounding suburban areas (Clinton & Gong, 2013; Peng et al., 2012), which was different from other regional or global analyses that took "rural" (certain distance away from urban) as reference locations (Imhoff et al., 2010; Tran et al., 2006; Zhang et al., 2010). Our SUHII definition can reduce the uncertainties associated with site-specific rural conditions across cities (e.g., topography, the presence of water body, and land use). In order to calculate SUHII, it is necessary to define and delineate urban and suburban areas on maps. The following steps were used to define urban and suburban areas:

(1) A built-up intensity (i.e., BI) map was generated from each urban coverage map using a 1 km × 1 km moving window method (to match the pixel size of MODIS LST data).
(2) A 50% threshold of BI was used as a criterion (e.g., Imhoff et al., 2010; Lu & Weng, 2006) to separate the BI maps into high- and low-intensity built-up land.

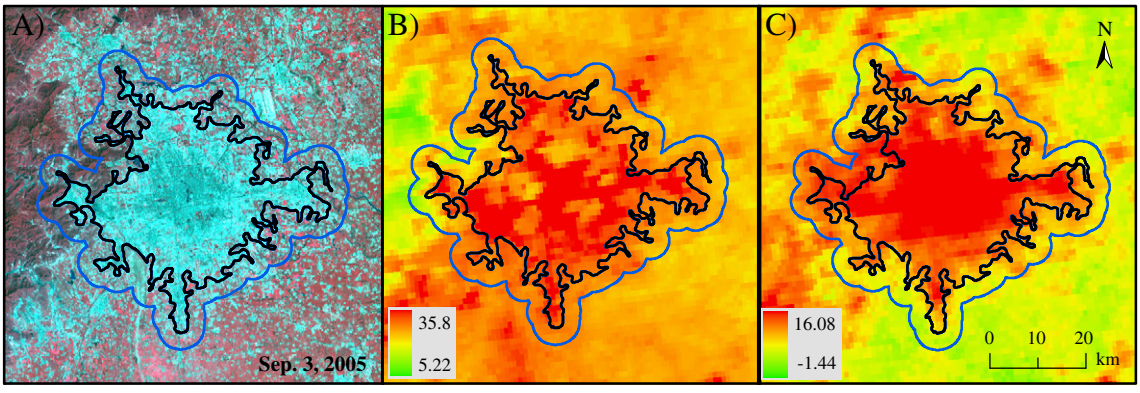

Fig. 2. The delineation of urban and suburban areas, an example of Beijing. Landsat TM false color image acquired in Sep 3, 2005 with a spatial resolution of 30 m × 30 m (A), and the annual mean land surface temperature (°C) during the day (B) and night (C) in 2005. The black line stands for the border of urban area, the land within the border was considered as the urban area, and that outside the black line but within the blue line represents the suburban area that covers the same amount of land as the urban area.

(3) The high-intensity built-up polygons were aggregated to delineate the urban border with an aggregation distance of 2 km, which is equivalent to two MODIS LST pixels and sufficient to include the scattered and most adjacent high-intensity built-up patches into the urban class. The land within the border was considered as urban area (excluding water pixels), which ranged from 47.6 km^2 (Lhasa) to as much as 2350.6 km^2 (Tianjin) in year 2010.
(4) A buffer zone around the urban area, exactly the same size as the urban area (excluding water pixels), was defined as the suburban area (Fig. 2).

We generated urban and suburban areas for each city map in 2000, 2005, and 2010. Since our timeframe of SUHII analysis was between 2003 and 2011, we assumed that the urban and suburban areas delineated in 2000, 2005, and 2010 can be used to represent those in 2003–2004, 2005–2009, and 2010–2011, respectively. The annual and seasonal (summer and winter) SUHII in the day (13:30) and night (1:30) were then calculated over the period 2003–2011 for each city individually. Summer and winter were defined as the periods from June to August, and from December to February, respectively. The diurnal SUHII amplitude (DSA) and the seasonal SUHII amplitude (SSA), defined as the SUHII differences between the day and night, and between summer and winter, respectively, were calculated to quantify the diurnal and seasonal SUHII amplitudes for each city. Finally, we estimated the annual and seasonal mean SUHII in all six regions across China during the day and night. To address the uncertainty introduced by the relatively small number of cities in each region, a nonparametric resampling procedure was used to generate bias-corrected bootstrap 95% confidence intervals of SUHIIs from 1000 randomizations of the observed SUHIIs within each region in SPSS PASW Statistics 18 (SPSS Inc.). Significance tests ($p = 0.05$) were then conducted to determine (1) if each of the estimated regional SUHII was statistically different from zero (i.e., does the SUHI exist?), (2) if there was a significant seasonal or diurnal difference in SUHII for each region, and (3) if there were differences in SUHII across regions.

In parallel with SUHII, five difference variables between urban and suburban pixels (i.e., vegetation index [ΔEVI], white sky albedo [ΔWSA], nighttime lights [ΔNL], elevation [ΔDEM], and built-up intensity [ΔBI]) and three fixed parameters (i.e., urban area size [UAS] and two climate factors [total precipitation and mean temperature]) were used to examine the possible drivers for the SUHII's spatial variations. The annual and seasonal ΔEVI, ΔWSA, total precipitation and mean temperature were calculated for each city over 2003–2011. In contrast, only annual ΔNL, ΔBI, ΔDEM, and UAS were estimated because there was no seasonal information available for them in our compiled database, thus were assumed the same during each season. To analyze plausible drivers that might control SUHII, a combination of correlation analysis, stepwise regression analysis, and our understanding on potential physical driving forces was adopted. The Pearson's correlation coefficients between the SUHII and the above-mentioned variables across cities were calculated using SPSS PASW Statistics 18 (SPSS Inc.). Stepwise multiple linear regressions were developed between SUHII and potential driving variables to find the best predictors and the independent explanation power of each selected variable to the spatial variation of SUHII.

3. Results

3.1. Spatial distributions of SUHII

Fig. 3 shows the spatial distribution of SUHII averaged over the period 2003–2011 for China's 32 major cities. The annual mean day and night SUHII averaged from 2003 to 2011 were positive in all the 32 cities varying from 0.01 (Lanzhou) to 1.87 °C (Shenyang) and 0.35 (Wuhan) to 1.95 °C (Shenyang), respectively (Fig. 3A and B). Overall, the cities located in the southeastern parts of China experienced more intense daytime SUHII (Northeast, East, Central-south, and Southwest China) than those in the North and the Northwest (Fig. 3A, Table 1). In contrast, the cities in the northern regions had higher nighttime SUHII (Northeast, North, and Northwest China) compared to their southern counterparts (East, Central-south, and Southwest China) (Fig. 3B, Table 1). Particularly, Northeast China, with humid-cold climate, exhibited the greatest SUHII in both day (1.43 [1.21, 1.65] °C, values in parenthesis define the 95% confidence interval, hereafter) and night (1.90 [1.84 to 1.95] °C). The annual mean diurnal SUHII amplitude (i.e., DSA) demonstrated a distinct spatial pattern (Fig. 3C, Table 1). It was positive in the East and the Central-south, close to zero in the Southwest, and negative in the northern parts of China.

The spatial patterns of SUHII differed greatly by season. In summer, the DSA was positive in all regions except the Northwest, and the largest DSA was found in the Northeast with 1.82 [1.47, 2.18] °C, followed by the East (1.38 [1.07, 1.69] °C) and Central-south (0.87 [0.50, 1.20] °C) (Fig. 3D, E, and F, Table 1). In contrast, the DSA was negative in all regions during the winter, but it was not statistically significant in the East and Central-south. The largest negative winter DSA occurred in the Northeast (−2.24 [−2.26, −2.21] °C), followed by the North (−2.11 [−2.53, −1.72] °C) and Northwest regions (−1.53 [−1.96, −1.13] °C) (Fig. 3G, H, and I, Table 1). A weak but statistically significant correlation between the daytime and nighttime SUHIIs was observed in summer ($r = 0.37$, $p < 0.05$), and no correlation was shown between them in winter ($r = -0.19$, $p = 0.30$) across cities. Meanwhile, an insignificant correlation and a strong correlation were illustrated between summer and winter SUHIIs during the day ($r = -0.17$, $p = 0.33$) and night ($r = 0.89$, $p < 0.01$), respectively (Fig. 4).

The seasonal SUHII amplitude (SSA) showed significant difference between day and night. The mean SSAs were 1.70 [1.35, 2.03] °C and −0.21 [-0.36, −0.08] °C, respectively, during the day and night for all 32 cities (Table 1). The large difference was resulted from the fact that the SUHII was more intense in summer than in winter for nearly all the cities (except Urumqi and Nanning) during the daytime (Fig. 3D, G and J, Table 1), and the opposite for most cities (23 of 32) at night (Fig. 3E, H and K, Table 1). Spatially, SSA was obviously higher in the day than that at night in all six regions (Fig. 3J and K, Table 1). The Northeast region had the largest SSA, closely followed by the North, and their SSAs were significantly larger than those in other regions for both day and night (Table 1).

3.2. Relationships between SUHII and potential drivers

The daytime SUHII correlated significantly and positively to the urban–suburban differences in nighttime lights (a proxy of anthropogenic heat releases) ($r = 0.65$, $p < 0.01$) and built-up intensity ($r = 0.40$, $p < 0.05$), negatively to the urban–suburban difference in enhanced vegetation index ($r = -0.59$, $p < 0.01$) in summer, and positively to precipitation ($r = 0.39$, $p < 0.05$) and temperature ($r = 0.35$, $p < 0.05$) in winter (Table 2). In contrast, the nighttime SUHII correlated significantly and positively to the urban–suburban differences of nighttime lights and built-up intensity, and negatively to the temperature and precipitation, and the urban–suburban difference of white sky albedo in both seasons.

Multiple stepwise regression analysis showed that the factors compiled in this analysis explained a significantly larger fraction of the SUHII variation at night compared to day and in winter relative to summer (night vs. day: 72% vs. 57% in summer, and 90% vs. 61% in winter, respectively) (Table 2). The daytime SUHII variation was primarily explained by nighttime lights (a proxy of anthropogenic heat releases) in summer (42%) and by climate (temperature and precipitation together 45%) in winter. Surface albedo accounted for most of the night SUHII variation regardless of season (i.e., 43% in summer and 65% in winter), and climate and anthropogenic heat releases explained significant portions of the variation as well.

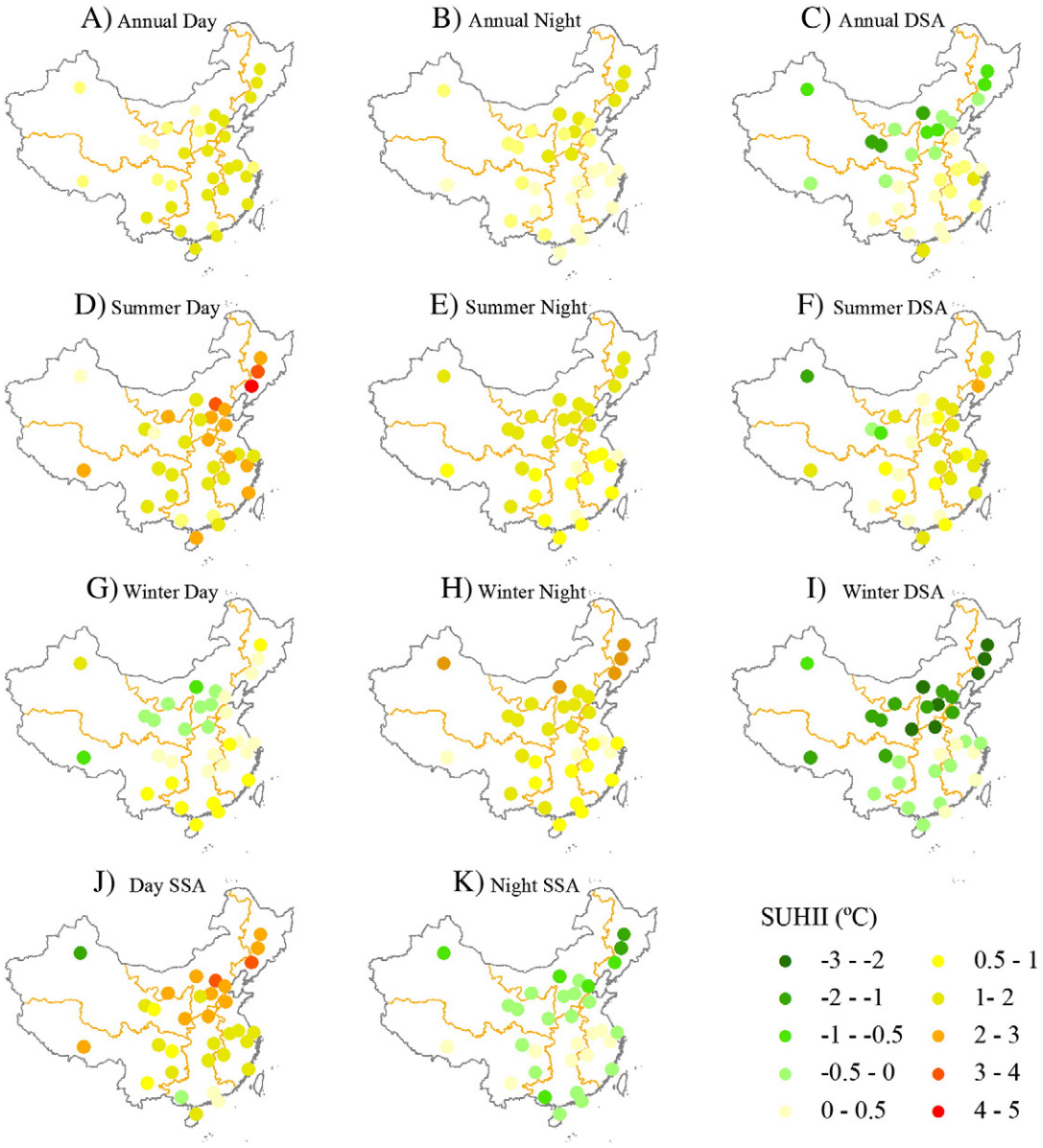

Fig. 3. Spatial distributions of surface urban heat island intensity (SUHII) in China's 32 major cities averaged over the period 2003–2011, including annual mean daytime SUHII (A), nighttime SUHII (B), diurnal SUHII amplitude (i.e., DSA) (C), and their seasonal counterparts during summer (D, E, and F) and winter (G, H, and I), respectively. The seasonal SUHII amplitude (i.e., SSA) during the day and night were illustrated in panels J and K, respectively. The DSA and SSA were defined as the SUHII differences between day and night, and between summer and winter, respectively.

4. Discussion

4.1. Possible mechanisms underlying SUHII spatial variability

Satellite thermal data reflect spatially aggregated heat information of the urban surface via upwelling thermal radiance that is received by remote sensors (Voogt & Oke, 2003). The resultant surface temperature was controlled by both surface radiative and thermodynamic properties. The surface energy balance can be expressed as: net all-wave radiation (R_n) + anthropogenic heat releases (F) = latent heat flux (LE) + sensible heat flux (H) + ground heat flux (ΔS) (Arnfield, 2003; Clinton & Gong, 2013). The SUHII in the day was broadly regarded as the consequence of a reduction in latent heat flux and an increase in sensible heat flux due to the rise of impervious surface at the expense of vegetated and evaporating soil surfaces (Arnfield, 2003; Clinton & Gong, 2013; Oke, 1982; Peng et al., 2012; Voogt & Oke, 2003), while that at night a result of more heat storage in urban zone during the day compared to surrounding areas (Clinton & Gong, 2013; Voogt & Oke, 2003). These effects can be indirectly exaggerated by the increasing anthropogenic heat emissions from traffic, industry, and domestic buildings (Arnfield, 2003; Yow, 2007). Factors influencing any heat component can alter the direction and/or magnitude of urban heat island during the day and/or night.

Our results indicated that the SUHII's spatial patterns in the day and night were driven by different variables (Fig. 4, Table 2), probably reflecting the variability of different heat fluxes in the dominance of the surface energy balance. For example, the latent and sensible heat fluxes dominate the energy balance equation in the day, whereas the ground heat fluxes become dominant at night (Arnfield, 2003; Clinton & Gong, 2013; Shepherd, 2005; Voogt & Oke, 2003). The driving mechanisms of the major biophysical and anthropogenic factors on SUHII effects (Table 2) are discussed separately below.

4.1.1. Vegetation activity

The presence of vegetation can increase the latent heat fluxes via transpiration (compared with impervious surfaces), and therefore was

Table 1
Mean effects (with 95% bootstrapped confidence intervals in parentheses based on 1000 bootstrap samples) of annual and seasonal (i.e., summer and winter) surface urban heat island intensity (SUHII, °C) during the day and night, as well as the diurnal and seasonal SUHII ranges across different regions of China averaged over the period 2003–2011. Diurnal SUHII amplitude (DSA) and seasonal SUHII amplitude (SSA) was defined as the SUHII difference between the day and night, and between summer and winter, respectively. Summer and winter were defined as the periods from June to August, and from December to February, respectively. *N* indicates the number of studied cities in each region.

Time		North ($N = 5$)	Northeast ($N = 3$)	East ($N = 7$)	Central-south ($N = 7$)	Southwest ($N = 5$)	Northwest ($N = 5$)	Total ($N = 32$)
Day	Summer	2.33 (1.88, 2.73)	3.36 (2.95, 3.77)	2.02 (1.66, 2.33)	1.57 (1.09, 2.02)	1.77 (1.48, 2.00)	1.22 (0.46, 2.04)	1.93 (1.66, 2.22)
	Winter	−0.25 (−0.55, −0.01)	0.39 (0.33, 0.45)	0.35 (0.15, 0.60)	0.50 (0.25, 0.71)	0.25 (−0.28, 0.76)	0.15 (−0.21, 0.54)	0.23 (0.05, 0.39)
	Annual	0.90 (0.51, 1.24)	1.43 (1.21, 1.65)	1.39 (1.17, 1.61)	1.24 (1.09, 1.40)	1.04 (0.75, 1.37)	0.66 (0.30, 1.09)	1.11 (0.97,1.25)
Night	Summer	1.45 (1.28, 1.59)	1.54 (1.43, 1.64)	0.64 (0.51, 0.80)	0.71 (0.52, 0.94)	0.94 (0.73, 1.17)	1.33 (1.20, 1.45)	1.02 (0.88, 1.16)
	Winter	1.86 (1.65, 2.02)	2.62 (2.58, 2.66)	0.55 (0.28, 0.85)	0.86 (0.57, 1.17)	0.88 (0.59, 1.25)	1.57 (1.31, 1.83)	1.23 (0.96, 1.49)
	Annual	1.61 (1.48, 1.75)	1.90 (1.84, 1.95)	0.70 (0.56, 0.91)	0.82 (0.57, 1.13)	0.94 (0.70, 1.17)	1.39 (1.21, 1.56)	1.13 (0.96, 1.30)
DSA	Summer	0.89 (0.44, 1.34)	1.82 (1.47, 2.18)	1.38 (1.07, 1.69)	0.87 (0.50, 1.20)	0.83 (0.53, 1.17)	−0.11 (−0.83, 0.62)	0.91 (0.66, 1.19)
	Winter	−2.11 (−2.53, −1.72)	−2.24 (−2.26, −2.21)	−0.20 (−0.60,0.16)	−0.37 (−0.90, 0.03)	−0.63 (−1.07, −0.18)	−1.53 (−1.96, −1.13)	−1.00 (−1.34, −0.68)
	Annual	−0.7 (−1.09, −0.40)	−0.47 (−0.68, −0.25)	0.68 (0.46, 0.91)	0.39 (0.05, 0.73)	0.08 (−0.12, 0.28)	−0.72 (−1.05, −0.39)	−0.02 (−0.25, 0.20)
SSA	Day	2.59 (2.15, 2.91)	2.97 (2.51, 3.44)	1.67 (1.41, 1.98)	1.08 (0.49, 1.78)	1.52 (0.99, 2.12)	1.18 (0.03, 2.26)	1.70 (1.35, 2.03)
	Night	−0.41 (−0.57, −0.25)	−1.09 (−1.19, −0.98)	0.09 (−0.11, 0.29)	−0.15 (−0.33, −0.01)	0.06 (−0.21, 0.28)	−0.24 (−0.46, −0.08)	−0.21 (−0.36, −0.08)

expected to generate a cooling effect on surface temperature and hence can mitigate SUHII effects (Li et al., 2011; Peng et al., 2012; Tran et al., 2006; Yuan & Bauer, 2007). The results in Table 2 support this mechanism because the difference in vegetation index between urban and suburban areas (i.e., ΔEVI) correlated negatively and strongly with daytime SUHII across cities in summer. Vegetation effect was insignificant in winter (Table 2) because of the low vegetation activities (e.g., the latent heat flux) in the season (Fig. 5C). Moreover, the seasonal change of ΔEVI was the best-predictor for the seasonal SUHII amplitude (i.e., SSA) in the day (Figs. 3J and 5D). The ΔEVI had insignificant correlations with nighttime SUHII in both seasons, which was expected owing primarily to the absence of transpiration during the night (Arnfield, 2003; Peng et al., 2012).

Unexpectedly, the indicator of vegetation activity (i.e., EVI) was not included in the stepwise multiple linear regression result to explain the SUHII variation. This suggested that the vegetation effects may be collinearly correlated with the effects of other factors that were in the regression. For example, the effects of vegetation were negatively and strongly coupled with the impacts of anthropogenic heat releases (as reflected by nighttime lights, $r = -0.59$, $p < 0.01$), an important independent variable in the regression equation.

4.1.2. Albedo

Urbanization generally decreases surface albedo and emissivity largely due to the urban "canopy effect" and the new materials used in urban roads or buildings. Together, they reduce heat loss through increased heat storage and net all-wave radiation in urban areas (Arnfield, 2003; Jin, Shepherd, et al., 2005; Oke, 1982; Stewart & Oke, 2012). Since the night SUHII was mainly driven by the surface heat fluxes that originated from heat storage during the day (Arnfield, 2003; Shepherd, 2005), the city with larger negative difference of albedo between urban and suburban areas (i.e., ΔWSA) was expected to have larger SUHII at night. This mechanism was verified by our findings that the night SUHII in both seasons was strongly correlated with ΔWSA (Table 2). Furthermore, the albedo effect was found more evident in winter compared to summer due to the greater ΔWSA (Fig. 6) resulted from vegetation defoliation and the presence of ice and snow in winter.

The impacts of urbanization on the surface albedo varied with region and its background vegetation. For instance, the Northeast, characterized by larch and seasonal cropland, exhibited the maximal negative ΔWSA along with high SUHII at night (Figs. 3B and C, and 6). In contrast, the southeastern cities, mainly covered by evergreen forests and continuous cropland, had small and positive values of ΔWSA that in part can explain the weak nighttime SUHII for those cities. These findings were similar to the results from Jin, Dickinson, and Zhang (2005) who suggested that the city surrounded by cropland and deciduous trees had larger albedo contrast between urban and suburban areas than that by evergreen forests.

4.1.3. Built-up intensity

Higher built-up intensity (i.e., BI) helps maintain warmer urban temperatures than lower BI since more heat can be trapped by street canyons, emitted by human activities, and stored by building materials, and less heat was lost because of the decreased vertical flux change (Oke, 1982; Yow, 2007). A larger BI difference between urban and suburban areas (i.e., ΔBI) was expected to have more intense SUHII in the city, in particular after the stored heat is released at night (Li et al., 2011; Tran et al., 2006; Yuan & Bauer, 2007). The significant positive correlations between ΔBI and nighttime SUHII observed in this study (Table 2) supported this mechanism. The overall ΔBI of the cities in the Northeast (i.e., Shenyang, Harbin, and Changchun) was larger than that in the other regions (data not shown), which at least partially contributed to the high SUHII in the region (Table 1).

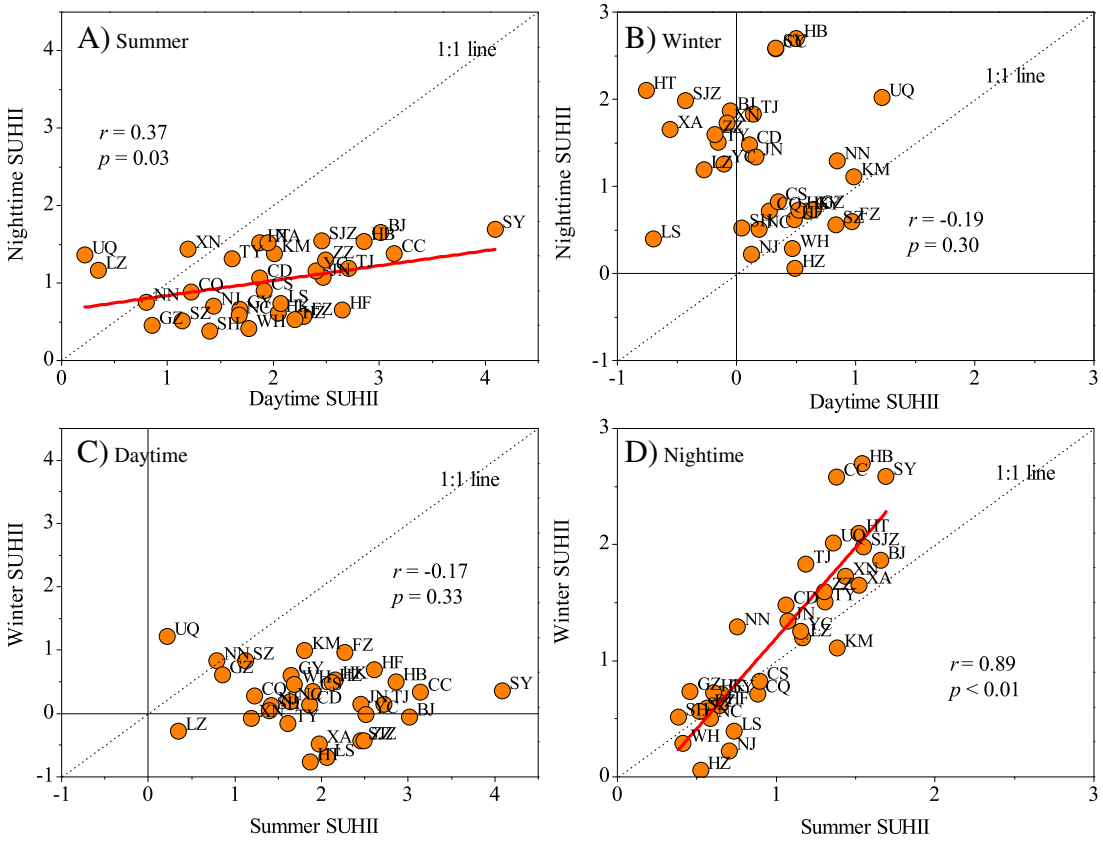

Fig. 4. Relationships of SUHII (°C) between the day and night during summer (A) and winter (B), and between summer and winter during the daytime (C) and nighttime (D) across China's 32 major cities averaged over the period 2003–2011. BJ: Beijing; CC: Changchun; CS: Changsha; CD: Chengdu; CQ: Chongqing; FZ: Fuzhou; GZ: Guangzhou; GY: Guiyang; HK: Haikou; HZ: Hangzhou; HB: Harbin; HF: Hefei; HT: Hohhot; JN: Jinan; KM: Kunming; LZ: Lanzhou; LS: Lhasa; NC: Nanchang; NJ: Nanjing; NN: Nanning; SH: Shanghai; SY: Shenyang; SZ: Shenzhen; SJZ: Shijiazhuang; TY: Taiyuan; TJ: Tianjin; UQ: Urumqi; WH: Wuhan; XA: Xi'an; XN: Xining; YC: Yinchuan; ZZ: Zhengzhou.

4.1.4. Anthropogenic heat emissions

The anthropogenic heat flux, which can be converted into sensible heat flux or other energy components (Christen & Vogt, 2004), influences the SUHII indirectly (Peng et al., 2012). Here we used the nighttime lights (i.e., NL) as a proxy for anthropogenic heat emissions (e.g., Amaral, Câmara, Monteiro, Quintanilha, & Elvidge, 2005; Peng et al., 2012). Results showed significantly positive correlations between ΔNL and SUHII in the day (for summer only) and at night (for both summer and winter) (Table 2). This positive relationship between ΔNL and SUHII was consistent with other studies (Peng et al., 2012; Yow, 2007).

4.1.5. Climate

Climatic condition was found to be a major reason for the observed SUHII spatial variability at night in both seasons and in the day in winter (Table 2). The negative impact of temperature on nighttime SUHII suggests that the cities located in cold and dry regions have a larger SUHII than those in hot and humid regions. This is different from the positive relationship found in single cities (e.g., Li et al., 2011; Tran et al., 2006). These results indicate that the relationship between SUHII and temperature across cities (spatial) is different from that for single cities (temporal), and that the concept of "replacing time by space" frequently used in ecological research (Pickett, 1989) is not applicable to studying the relationship between SUHII and climate.

Climate effects can be explained more directly by soil moisture difference (Oke, 1982; Oke, Johnson, Steyn, & Watson, 1991; Tran et al., 2006). The hot–wet cities (i.e., the southern and eastern regions) normally had higher soil moisture content than cold–dry cities (i.e., the Northwest) (Chow & Roth, 2006). Consequently, the hot–wet cities

Table 2
Pearson's correlation coefficients between the SUHII's fluctuations and driving variables and the independent explanation rate (%) of each variable derived from stepwise multiple linear regressions (in parentheses). EVI, enhanced vegetation index; WSA, white-sky albedo; NL, nighttime lights; BI, built-up intensity, defined as the percentage of landscape taken by built-up land; UAS, urban area size (logarithmic transformed); MT, mean temperature; TP, total precipitation;Δ indicates the difference between the urban and suburban areas. All the factors were considered the same over the day and night. The factors including ΔWSA, ΔEVI, MT and TP were grouped by season, but the other variables (i.e., ΔNL, ΔBI, ΔDEM and UAS) were assumed the same in spite of season because there was no seasonal information of them in our compiled database.

Variables		ΔEVI	ΔWSA	ΔNL	ΔBI	ΔDEM	UAS	MT	TP	Combined
Day	Summer	−0.59[a] (6)	−0.06 (4)	0.65[a] (42[a])	0.40[b] (1)	0.06 (2)	0.33	−0.05	−0.25 (2)	– (57)
	Winter	−0.28 (1)	−0.1 (10)	−0.18 (2)	0.01 (2)	0.23	0 (1)	0.35[b] (30[a])	0.39[b] (15[b])	– (61)
Night	Summer	−0.34 (4)	−0.67[a] (43[a])	0.59[a] (12[a])	0.44[b]	−0.25 (2)	0.14 (1)	−0.52[a] (4)	−0.63[a] (7[b])	– (72)
	Winter	0.21 (1)	−0.81[a] (65[a])	0.71[a] (2[b])	0.45[b] (1)	−0.1	0.25 (5[a])	−0.69[a] (3[a])	−0.65[a] (12[a])	– (90)

[a] significant at the 0.01 level; [b] significant at the 0.05 level.

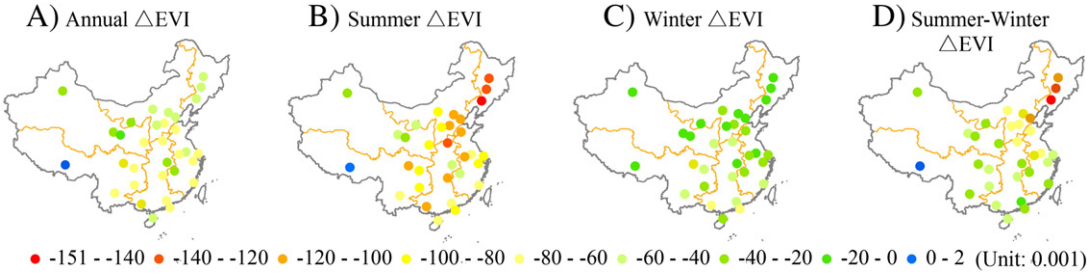

Fig. 5. Spatial distributions of the annual (A), summer (B), winter (C), and seasonal amplitudes (Summer–Winter) (D) of the urban–suburban differences in enhanced vegetation index (ΔEVI) across China's 32 major cities averaged over the period 2003–2011.

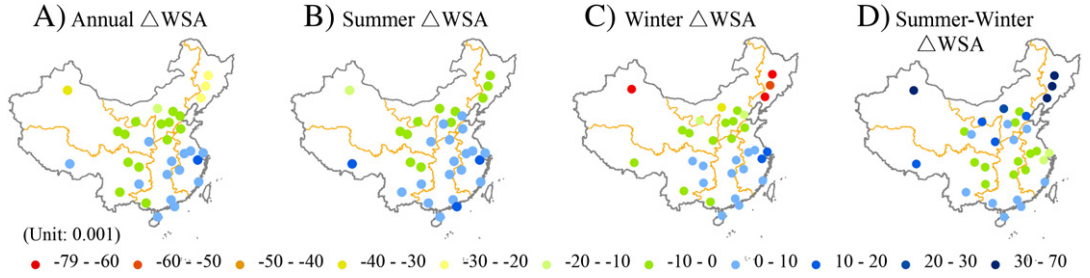

Fig. 6. Spatial distributions of the annual (A), summer (B), winter (C), and seasonal changes (Summer–Winter) (D) of the urban–suburban differences in White Sky Albedo (ΔWSA) across China's 32 major cities averaged over the period 2003–2011.

generally promote larger urban–suburban difference in soil moisture than cold-dry cities, resulting in higher daytime and lower nighttime LST differences between urban and suburban areas (i.e., SUHII) and thus larger SUHII differences between day and night (i.e., DSA). For example, the East (with humid-hot climate) had an annual mean DSA of 0.68 [0.46, 0.91] °C, whereas the Northwest (with arid-cold climate) had a negative DSA of −0.72 [−1.09, −0.40] °C (Table 1). In addition, climate indirectly affect SUHII through regulating vegetation conditions (Piao et al., 2003), surface albedo (Hall, 2004), and anthropogenic heat emissions (Santamouris et al., 2001). For instance, we found that the mean temperature correlated significantly with enhanced vegetation index ($r = -0.66$, $p < 0.01$), surface albedo ($r = 0.74$, $p < 0.01$), and nighttime lights ($r = -0.64$, $p < 0.01$) in winter across cities (Fig. 7).

4.1.6. City size and topography

Many previous studies found that the SUHII increased with city sizes (Imhoff et al., 2010; Nichol, 1996; Streutker, 2002). In addition, the SUHII should change with the urban–suburban difference in elevation (ΔDEM) because of the orographic effect. This study did not reveal significant relationship between SUHII and either of the factors (Table 2). The small variations of city topography between urban and suburban areas for most cities (i.e., the mean ΔDEM of all cities was −13 m) was not enough to cause any elevation impact.

4.1.7. Combined effects

Overall, the factors integrated in this study explained a greater portion of the SUHII's spatial variations at night compared to the day and in winter relative to summer (Table 2). The joint explanatory power of these drivers ranged from 57% during the day in summer to 90% during the night in winter, suggesting more complicated mechanisms underlying the daytime SUHII's spatial patterns (particularly in summer), and that other factors, such as landscape configuration, atmospheric environment, and land use (Jáuregui & Luyando, 1999; Li et al., 2011; Oke, 1982), may play important roles. Previous studies suggested that vegetation largely determines the daytime SUHII distribution in summer (Li et al., 2011; Peng et al., 2012; Tran et al., 2006; Yuan & Bauer, 2007). Our results indicated that anthropogenic heat emissions, which was significantly related to vegetation activity, explained most of the

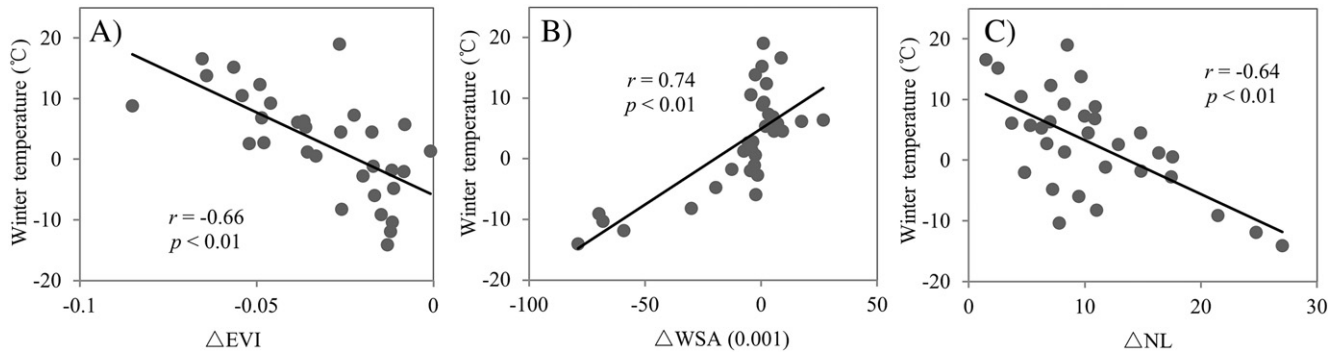

Fig. 7. Correlations between the temperature and ΔEVI, ΔWSA, or ΔNL in winter across China's 32 major cities averaged over the period 2003–2011.

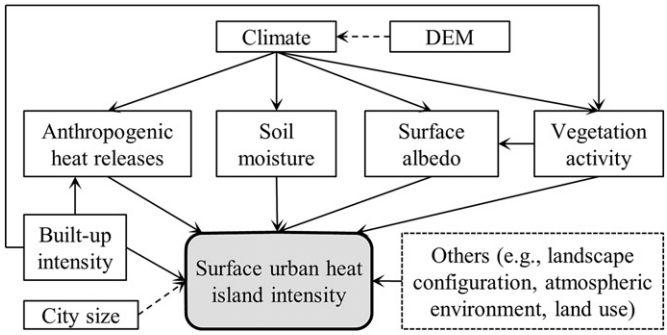

Fig. 8. Conceptual diagram illustrating the possible driving forces of the SUHII spatial variability. Dashed line indicates an insignificant correlation with SUHII according to this analysis.

SUHII spatial variability during the day in summer, while climate explained the most daytime SUHII variability in winter. The albedo contributed most to the nighttime SUHII's fluctuations regardless of season (Table 2), which was consistent with the findings from Peng et al. (2012) at global scale. The impact of vegetation did not show up in the stepwise regressions directly, suggesting more detailed research is needed to disentangle direct and indirect effects of vegetation on SUHII.

Climate might be the ultimate factor that defines the spatial pattern of SUHII over large areas, and the impacts of most other factors (e.g., vegetation and anthropogenic heat fluxes) might largely reflect the climate effects (Fig. 8). Both diurnal and seasonal SUHIIs showed similar patterns in each climate region (Fig. 3), which signifies the ultimate effect of climate on the SUHII variations. The climate control can be shown more clearly by the strong relationship between the diurnal SUHII amplitude (DSA) and precipitation ($r = 0.83$, $p < 0.01$) or temperature ($r = 0.76$, $p < 0.01$) (Fig. 9). For the cities with similar climate conditions, other anthropogenic factors such as built-up intensity may play important roles. For example, the nighttime SUHII in the cities of East, Central-south, and Southwest China (with humid hot climates) related closely and positively to the ΔBI in both summer ($r = 0.71$, $p < 0.01$) and winter ($r = 0.54$, $p < 0.05$). City size, however, exhibited insignificant relationship with the SUHII across cities even in the same climate region.

4.2. Spatial patterns of SUHII in China and their drivers

Because of the possible different driving forces, the spatial pattern of the annual mean daytime SUHII was different from that of nighttime (Fig. 3). In the daytime, the annual mean SUHII was apparently weaker in arid cities (Fig. 3A, Table 1), mostly owing to the shorter and sparser

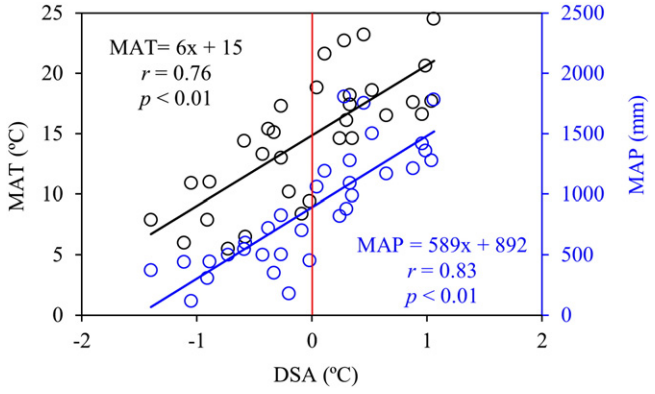

Fig. 9. Relationships between the mean annual temperature (MAT) or mean annual precipitation (MAP) and the diurnal SUHII amplitude (DSA) across China's 32 major cities averaged over the period 2003–2011.

vegetation in their suburban areas compared to other regions (Fig. 5A). For example, both the mean annual daytime SUHII and ΔEVI in the Northwest were only half of those in the Central-south, respectively (Table 1 and Fig. 5A). Similar observations were reported in other regions around the world (Imhoff et al., 2010; Peña, 2008; Peng et al., 2012). In contrast, low annual night SUHII was found in the southeastern regions (Fig. 3B, Table 1), which can be explained by their high soil moisture (induced by the humid-hot climate) and the low surface albedo in the suburban areas (Fig. 6A). Shenyang witnessed the most intense SUHII across cites, which can be mainly attributed to the highest EVI (in summer) and WSA differences between urban and suburban areas of the city (Figs. 5 and 6) together with its relatively high built-up intensity.

Large seasonal changes of SUHII with evident spatial distributions were observed for the 32 cities. In the daytime, the SUHII was more intense in summer than in winter for nearly all the cities (Figs. 3F and 4C), mainly because of the stronger evaporative cooling effects produced by vegetation over suburbs in summer than in winter (Fig. 5D) (Imhoff et al., 2010; Jin, 2012; Tran et al., 2006). In particular, the Northeast, with humid-cold climate, witnessed the largest seasonal SUHII amplitude (Fig. 3J, Table 1), which might be caused by its seasonal change of vegetation activity, also the largest among all regions, characterized by intensive agricultural practices in summer and defoliation in winter (Piao et al., 2003). Conversely, the SUHII was weaker in summer than in winter for most of the cities during the nighttime, particularly in the northern regions (Figs. 3K and 4D). Three factors might contribute to this phenomenon. First, the albedo differences between urban and suburbs were more pronounced during winter than summer because of defoliation and/or snow and ice coverage for most cities, particularly for the high-latitude cities (Fig. 6D), which in turn increase the night SUHII in winter (Table 2). Second, lower soil moisture in winter than in summer over most regions, influenced by the monsoon climate (Wu et al., 2005), could drive a larger nighttime SUHII in winter than in summer (Table 2) through reducing heat storage and subsequent release at night in the suburban zones. Finally, the heating-created anthropogenic heat flux in urban areas during winter, especially for the high-latitude cities where central heating systems are used extensively, can indirectly strengthen SUHII.

Our results showed that whether the day SUHII for a city is higher than the night SUHII depends strongly on the climate region and time period, suggesting caution when interpreting and extrapolating results. For example, Imhoff et al. (2010) and Peng et al. (2012) concluded that the annual mean SUHII was larger in the day than at night across big cities at regional and global levels. However, our results differed from these studies showing the overall annual mean daytime and nighttime SUHII were roughly equal across 32 cities (Table 1). This can be attributed to the difference in the distributions of the cities across climate regions. Two observations from this study further confirmed the importance of climate zones. First, the annual mean SUHII was higher in the day than at night when the cities in the humid coastal regions were examined only (Fig. 3C), similar to the findings from Imhoff et al. (2010) and Peng et al. (2012). Second, the annual mean SUHII demonstrated a strong variability across different climate regions of China (Fig. 3A and B), suggesting the change of research region can lead different results. In addition, the characteristics of SUHII vary greatly with season as well. For example, a higher SUHII in summer than in winter was most likely observed for the day, with the opposite for the night (Fig. 4A and B). It is therefore necessary to realize the empirical nature of the observed large-scale SUHII's patterns because of their dependence on space and time.

4.3. Uncertainties and suggestions

Uncertainties existed in the SUHII's distributions in this analysis. First, a negative daytime SUHII was observed in some northern or northwestern cities during winter (Fig. 3G). The reason for this unexpected

phenomenon was not clear, but might be related to the atmospheric environments. For example, the air pollution, peaked in winter for most cities in China especially for the northern cities because of the large amount of coal burned for heating (He, Huo, & Zhang, 2002) and the impacts were not corrected in the MODIS LST products (Wan, 2008), decreased the incoming short wave solar radiation in urban areas relative to surrounding suburbs (Sang, Liu, Liu, & Zhang, 2000), which might artificially result in a negative SUHII. Second, a large fraction of the daytime SUHII fluctuations (43% in summer and 39% in winter) remained unexplained by the drivers included in current research (Table 2). These two issues highlighted the importance of considering more variables in future SUHII studies, such as landscape configuration (Arnfield, 2003; Li et al., 2011; Oke, 1982), atmospheric environment (Jáuregui & luyando, 1999), land use, the presence of water bodies, and the nature of soils (Jin, Dickinson, et al., 2005; Morris, Simmonds, & Plummer, 2001; Oke, 1982). Third, there are multicollinearity problems among different factors, and multiple statistical techniques might be needed to enhance the reliability and interpretation of the driving forces. Fourth, we used dynamic urban coverage maps to delineate urban and suburban areas for each city in this study in order to reflect the actual SUHII situations impacted by rapid urban expansion. For example, the urban areas for the 32 major Chinese cities increased by 1.3 times on average between 2000 and 2010. This stressed the necessity of a more detailed work to quantify the possible SUHII biases induced by using the static urban coverage map as most previous studies did (e.g., Clinton & Gong, 2013; Imhoff et al., 2010; Peng et al., 2012) in future.

Despite the above uncertainties, this study confirmed the importance of vegetation in mitigating SUHII during the daytime in summer as advocated by many previous studies (e.g., Li et al., 2011; Peng et al., 2012; Yuan & Bauer, 2007). Beyond that, we recommend that more attention should be paid to the other climate mitigation actions, such as an increase in urban surface albedo and a reduction in anthropogenic heat emissions. For example, we can increase urban surface albedo using solar-reflective materials and landscape configuration, and decrease anthropogenic heat emissions by promoting energy-saving consciousness and products (Arnfield, 2003; Jin, Shepherd, et al., 2005; Li et al., 2011; Oke, 1982).

5. Conclusions

This study analyzed the diurnal and seasonal SUHIIs in 32 major cities across different regions of China. Because China is characterized by complex zonal variations, this research provides valuable information on assessing urban heat island at regional scale. Our results indicated the SUHII differed substantially between day and night, with distinct climate-driven patterns, characterized by a higher SUHII in the southeastern parts of China in the day, and in the northern regions of the country at night compared with other regions. In particular, the Northeast, with humid-cold climate, experienced the most intense SUHII across China. In addition, the SUHII varied greatly with season, indicated by a relatively higher intensity in the day for the summer and at night for winter across most cities. As a result, whether the daytime SUHII was higher or lower than the nighttime SUHII depends strongly on the climate region and time period investigated.

The SUHII distribution in the day correlated significantly to vegetation activity and anthropogenic heat emissions in summer and to climate in winter, and at night was related closely to surface albedo, anthropogenic heat emissions, built-up intensity, and climate in both seasons. Overall, climate showed ultimate control on the SUHII spatial variability. A much smaller fraction of the SUHII variations was explained by the factors included in this study in the day compared to night and in summer relative to winter (day vs. night: 57% vs. 72% in summer, and 61% vs. 90% in winter, respectively), indicating more complicated mechanisms underlying the spatial patterns of SUHII in the daytime, especially in summer. Our results highlight the different diurnal (day and night) and seasonal (summer and winter) SUHII's spatial patterns and the underlying mechanisms, suggesting caution when extrapolating results across space and time without complex modeling. To mitigate UHI effects, we recommend that efforts should be targeted to increase urban vegetation activity and surface albedo, and reduce anthropogenic heat emissions.

Acknowledgements

This study was supported by the National Natural Science Foundation of China (#31321061 and #41071050), the QianRen Program, and the Innovation Teams Program of Hunan Natural Science Foundation of China (2013 #7).

Appendix A. Supplementary data

Supplementary data associated with this article can be found in the online version, at http://dx.doi.org/10.1016/j.rse.2014.05.017. These data include Google map of the most important areas described in this article.

References

Amaral, S., Câmara, G., Monteiro, A.M. V., Quintanilha, J. A., & Elvidge, C. D. (2005). Estimating population and energy consumption in Brazilian Amazonia using DMSP night-time satellite data. *Computers, Environment and Urban Systems*, *29*, 179–195.
Arnfield, A. J. (2003). Two decades of urban climate research: a review of turbulence, exchanges of energy and water, and the urban heat island. *International Journal of Climatology*, *23*, 1–26.
Cai, G., Du, M., & Xue, Y. (2011). Monitoring of urban heat island effect in Beijing combining ASTER and TM data. *International Journal of Remote Sensing*, *32*(5), 1213–1232.
Chow, W. T. L., & Roth, M. (2006). Temporal dynamics of the urban heat island of Singapore. *International Journal of Climatology*, *26*, 2243–2260.
Christen, A., & Vogt, R. (2004). Energy and radiation balance of a central European city. *International Journal of Climatology*, *24*, 1395–1421.
Clinton, N., & Gong, P. (2013). MODIS detected surface urban heat islands and sinks: Global locations and controls. *Remote Sensing of Environment*, *134*, 294–304.
Ding, H., & Shi, W. (2013). Land-use/land-cover change and its influence on surface temperature: a case study in Beijing City. *International Journal of Remote Sensing*, *34*, 5503–5517.
Dixon, P. G., & Mote, T. L. (2003). Patterns and causes of Atlanta's urban heat island-initiated precipitation. *Journal of Applied Meteorology*, *42*, 1273–1284.
Elvidge, C. D., Imhoff, M. L., Baugh, K. E., Hobson, V. R., Nelson, I., Safran, J., et al. (2001). Night-time lights of the world: 1994–1995. *ISPRS Journal of Photogrammetry and Remote Sensing*, *56*, 81–99.
Fang, J., Chen, A., Peng, C., Zhao, S., & Ci, L. (2001). Changes in forest biomass carbon storage in China between 1949 and 1998. *Science*, *292*, 2320–2322.
Fast, J.D., Torcolini, J. C., & Redman, R. (2005). Pseudovertical temperature profiles and the urban heat island measured by a temperature datalogger network in Phoenix, Arizona. *Journal of Applied Meteorology*, *44*, 3–13.
Foody, G. M. (2002). Status of land cover classification accuracy assessment. *Remote Sensing of Environment*, *80*(1), 185–201.
Ghosh, T., Powell, R. L., Elvidge, C. D., Baugh, K. E., Sutton, P. C., & Anderson, S. (2010). Shedding light on the global distribution of economic activity. *The Open Geography Journal*, *3*, 148–161.
Gong, P., Liang, S., Carlton, E. J., Jiang, Q., Wu, J., Wang, L., et al. (2012). Urbanisation and health in China. *The Lancet*, *379*, 843–852.
Grimm, N.B., Faeth, S. H., Golubiewski, N. E., Redman, C. L., Wu, J., Bai, X., et al. (2008). Global change and the ecology of cities. *Science*, *319*, 756–760.
Hall, A. (2004). The role of surface albedo feedback in climate. *Journal of Climate*, *17*, 1550–1568.
He, K., Huo, H., & Zhang, Q. (2002). Urban air pollution in China: current status, characteristics, and progress. *Annual Review of Energy and the Environment*, *27*, 397–431.
Imhoff, M. L., Bounoua, L., DeFries, R., Lawrence, W. T., Stutzer, D., Tucker, C. J., et al. (2004). The consequences of urban land transformation on net primary productivity in the United States. *Remote Sensing of Environment*, *89*, 434–443.
Imhoff, M. L., Zhang, P., Wolfe, R. E., & Bounoua, L. (2010). Remote sensing of the urban heat island effect across biomes in the continental USA. *Remote Sensing of Environment*, *114*, 504–513.
IPCC (Intergovernmental Panel on Climate Change) (2007). *Climate Change 2007 Synthesis Report*. New York: Cambridge University Press.
Jáuregui, E., & Luyando, E. (1999). Global radiation attenuation by air pollution and its effects on the thermal climate in Mexico City. *International Journal of Climatology*, *19*, 683–694.
Jin, M. S. (2012). Developing an index to measure urban heat island effect using satellite land skin temperature and land cover observations. *Journal of Climate*, *25*, 6193–6201.
Jin, M., Dickinson, R. E., & Zhang, D. (2005). The footprint of urban areas on global climate as characterized by MODIS. *Journal of Climate*, *18*, 1551–1565.

Jin, M., Shepherd, J. M., & King, M.D. (2005b). Urban aerosols and their variations with clouds and rainfall: A case study for New York and Houston. *Journal of Geophysical Research*, *110*, D10S20. http://dx.doi.org/10.1029/2004JD005081.
Karl, T. R., & Quayle, R. G. (1988). Climate change in fact and in theory: Are we collecting the facts? *Climatic Change*, *13*, 5–17.
Li, J., Song, C., Cao, L., Zhu, F., Meng, X., & Wu, J. (2011). Impacts of landscape structure on surface urban heat islands: A case study of Shanghai, China. *Remote Sensing of Environment*, *115*, 3249–3263.
Lu, D., & Weng, Q. (2006). Use of impervious surface in urban land-use classification. *Remote Sensing of Environment*, *102*, 146–160.
McCarthy, M. P., Best, M. J., & Betts, R. A. (2010). Climate change in cities due to global warming and urban effects. *Geophysical Research Letters*, *37*, L09705. http://dx.doi.org/10.1029/2010GL042845.
Morris, C., Simmonds, I., & Plummer, N. (2001). Quantification of the influences of wind and cloud on the nocturnal urban heat island of a large city. *Journal of Applied Meteorology*, *40*, 169–182.
Nichol, J. E. (1996). High-resolution surface temperature patterns related to urban morphology in a tropical city: A satellite-based study. *Journal of Applied Meteorology*, *35*, 135–146.
O'Loughlin, J., Witmer, F. D. W., Linke, A.M., Laing, A., Gettelman, A., & Dudhia, J. (2012). Climate variability and conflict risk in East Africa, 1990–2009. *Proceedings of the National Academy of Sciences of the United States of America*, *109*, 18344–18349.
Oke, T. R. (1973). City size and the urban heat island. *Atmospheric Environment*, *7*, 769–779.
Oke, T. R. (1982). The energetic basis of the urban heat island. *Quarterly Journal of the Royal Meteorological Society*, *108*, 1–24.
Oke, T. R., Johnson, G. T., Steyn, D.G., & Watson, I. D. (1991). Simulation of surface urban heat islands under 'ideal' conditions at night Part 2: Diagnosis of causation. *Boundary-Layer Meteorology*, *56*, 339–358.
Patz, J. A., Campbell-Lendrum, D., Holloway, T., & Foley, J. A. (2005). Impact of regional climate change on human health. *Nature*, *438*, 310–317.
Peña, M.A. (2008). Relationships between remotely sensed surface parameters associated with the urban heat sink formation in Santiago, Chile. *International Journal of Remote Sensing*, *29*, 4385–4404.
Peng, S., Piao, S., Ciais, P., Friedlingstein, P., Ottle, C., Bréon, F. M., et al. (2012). Surface urban heat island across 419 global big cities. *Environmental Science & Technology*, *46*, 696–703.
Peterson, T. C. (2003). Assessment of urban versus rural in situ surface temperatures in the contiguous United States: No difference found. *Journal of Climate*, *16*, 2941–2959.
Piao, S., Fang, J., Zhou, L., Guo, Q., Henderson, M., Ji, W., et al. (2003). Interannual variations of monthly and seasonal normalized difference vegetation index (NDVI) in China from 1982 to 1999. *Journal of Geophysical Research*, *108*, 4401. http://dx.doi.org/10.1029/2002JD002848 (D14).
Pickett, S. T. (1989). Space-for-time substitution as an alternative to long-term studies. *Long-term studies in ecology* (pp. 110–135). New York: Springer.
Reid, W. V. (1998). Biodiversity hotspots. *Trends in Ecology & Evolution*, *13*, 275–280.
Rigo, G., Parlow, E., & Oesch, D. (2006). Validation of satellite observed thermal emission with in-situ measurements over an urban surface. *Remote Sensing of Environment*, *104*, 201–210.
Sang, J., Liu, H., Liu, H., & Zhang, Z. (2000). Observational and numerical studies of wintertime urban boundary layer. *Journal of Wind Engineering and Industrial Aerodynamics*, *87*, 243–258.
Santamouris, M., Papanikolaou, N., Livada, I., Koronakis, I., Georgakis, C., Argiriou, A., et al. (2001). On the impact of urban climate on the energy consumption of buildings. *Solar Energy*, *70*, 201–216.
Shepherd, J. M. (2005). A review of current investigations of urban-induced rainfall and recommendations for the future. *Earth Interactions*, *9*, 1–27.
Stewart, I. D., & Oke, T. R. (2012). Local Climate Zones for Urban Temperature Studies. *Bulletin of the American Meteorological Society*, *93*(12), 1879–1900.
Strahler, A. H. (1980). The use of prior probabilities in maximum likelihood classification of remotely sensed data. *Remote Sensing of Environment*, *10*, 135–163.
Streutker, D. R. (2002). A remote sensing study of the urban heat island of Houston, Texas. *International Journal of Remote Sensing*, *23*, 2595–2608.
Tran, H. D., Uchihama, S. O., & Yasuoka, Y. (2006). Assessment with satellite data of the urban heat island effects in Asian mega cities. *International Journal of Applied Earth Observation and Geoinformation*, *8*(1), 34–48.
Vitousek, P.M., Mooney, H. A., Lubchenco, J., & Melillo, J. M. (1997). Human domination of Earth's ecosystems. *Science*, *277*(5325), 494–499.
Voogt, J. A., & Oke, T. R. (2003). Thermal remote sensing of urban climates. *Remote Sensing of Environment*, *86*, 370–384.
Wan, Z. (2008). New refinements and validation of the MODIS land-surface temperature/emissivity products. *Remote Sensing of Environment*, *112*, 59–74.
Wan, Z., & Dozier, J. (1996). A generalized split-window algorithm for retrieving land-surface temperature from space. *IEEE Transactions on Geoscience and Remote Sensing*, *34*, 892–905.
Wu, S., Yin, Y., Zheng, D., & Yang, Q. (2005). Aridity/humidity status of land surface in China during the last three decades. *Science in China Series D: Earth Sciences*, *48*, 1510–1518.
Xu, H., & Chen, B. (2004). Remote sensing of the urban heat island and its changes in Xiamen City of SE China. *Journal of Environmental Sciences*, *16*, 276–281.
Yow, D.M. (2007). Urban heat islands: observations, impacts, and adaptation. *Geography Compass*, *1*, 1227–1251.
Yuan, F., & Bauer, M. E. (2007). Comparison of impervious surface area and normalized difference vegetation index as indicators of surface urban heat island effects in Landsat imagery. *Remote Sensing of Environment*, *106*, 375–386.
Zhang, P., Imhoff, M. L., Wolfe, R. E., & Bounoua, L. (2010). Characterizing urban heat islands of global settlements using MODIS and nighttime lights products. *Canadian Journal of Remote Sensing*, *36*, 185–196.
Zhou, D. C., Zhao, S. Q., & Zhu, C. (2012). The Grain for Green Project induced land cover change in the Loess Plateau: A case study with Ansai County, Shanxi Province, China. *Ecological Indicators*, *23*, 88–94.